Acta Crystallographica Section D
Biological Crystallography
ISSN 1399-0047

Structural insights into the substrate specificity and transglycosylation activity of a fungal glycoside hydrolase family 5 β-mannosidase

Peng Zhou,[a]‡ Yang Liu,[b]‡ Qiaojuan Yan,[c] Zhongzhou Chen,[b] Zhen Qin[a] and Zhengqiang Jiang[a]*

[a]Department of Biotechnology, College of Food Science and Nutritional Engineering, China Agricultural University, Beijing 100083, People's Republic of China, [b]State Key Laboratory of Agrobiotechnology, College of Biological Sciences, China Agricultural University, Beijing 100193, People's Republic of China, and [c]Bioresource Utilization Laboratory, College of Engineering, China Agricultural University, Beijing 100083, People's Republic of China

‡ These authors contributed equally to this work.

Correspondence e-mail: zhqjiang@cau.edu.cn

Received 14 April 2014
Accepted 2 September 2014

PDB references: *Rm*Man5A, 4qp0; *Rm*Man5B, 4lyp; *Rm*Man5B/E202A, mannobiose complex, 4nrs; *Rm*Man5B/E202A, mannotriose complex, 4lyq; *Rm*Man5B/E202A, mannosyl-fructose complex, 4nrr; *Rm*Man5B/E301A, 4lyr

β-Mannosidases are exo-acting glycoside hydrolases (GHs) that catalyse the removal of the nonreducing end β-D-mannose from manno-oligosaccharides or mannoside-substituted molecules. They play important roles in fundamental biological processes and also have potential applications in various industries. In this study, the first fungal GH family 5 β-mannosidase (*Rm*Man5B) from *Rhizomucor miehei* was functionally and structurally characterized. *Rm*Man5B exhibited a much higher activity against manno-oligosaccharides than against *p*-nitrophenyl β-D-mannopyranoside (*p*NPM) and had a transglycosylation activity which transferred mannosyl residues to sugars such as fructose. To investigate its substrate specificity and transglycosylation activity, crystal structures of *Rm*Man5B and of its inactive E202A mutant in complex with mannobiose, mannotriose and mannosyl-fructose were determined at resolutions of 1.3, 2.6, 2.0 and 2.4 Å, respectively. In addition, the crystal structure of *R. miehei* β-mannanase (*Rm*Man5A) was determined at a resolution of 2.3 Å. Both *Rm*Man5A and *Rm*Man5B adopt the $(\beta/\alpha)_8$-barrel architecture, which is globally similar to the other members of GH family 5. However, *Rm*Man5B shows several differences in the loop around the active site. The extended loop between strand β8 and helix α8 (residues 354–392) forms a 'double' steric barrier to 'block' the substrate-binding cleft at the end of the −1 subsite. Trp119, Asn260 and Glu380 in the β-mannosidase, which are involved in hydrogen-bond contacts with the −1 mannose, might be essential for exo catalytic activity. Moreover, the structure of RmMan5B in complex with mannosyl-fructose has provided evidence for the interactions between the β-mannosidase and D-fructofuranose. Overall, the present study not only helps in understanding the catalytic mechanism of GH family 5 β-mannosidases, but also provides a basis for further enzymatic engineering of β-mannosidases and β-mannanases.

1. Introduction

Mannans are important constituents of higher plant cell walls, and also display a storage function as nonstarch carbohydrate reserves in vegetative tissues. They are the dominant constituents of hemicelluloses, which represent the second most abundant source of organic carbon within the biosphere (Moreira & Filho, 2008). Mannans have been classified into two major groups depending on whether the β-1,4-linked backbone contains only D-mannose residues (mannans) or a combination of mannose and D-glucose residues (glucomannans). Each of these groups can be subdivided based on the number of α-1,6-linked galactose side groups (galactomannans and galactoglucomannans; Van Zyl *et al.*, 2010). Owing to their complex structures, the mannan-degrading enzymes are composed of β-mannanase (EC 3.2.1.78),

β-mannosidase (EC 3.2.1.25), β-glucosidase (EC 3.2.1.21), α-galactosidase (EC 3.2.1.23) and acetyl mannan esterase (EC 3.1.1.6) (Moreira & Filho, 2008). As an exo-type enzyme, β-mannosidase cleaves β-1,4-linked mannosides and releases mannose from the nonreducing end of mannans and manno-oligosaccharides. β-Mannosidases together with β-mannanases are widely used in various industries such as the food, feed, biofuel, pulp and paper industries (Dhawan & Kaur, 2007). In addition, β-mannosidases have potential applications in the synthesis of oligosaccharides for medical and other purposes (Eneyskaya *et al.*, 2009; Zhang *et al.*, 2009).

Based on amino-acid sequence similarity, glycoside hydrolases (GHs) have been classified into 133 families (http://www.cazy.org/; Lombard *et al.*, 2014). To date, all reported β-mannanases and β-mannosidases belong to GH families 1, 2, 5, 26 and 113. β-Mannanases are classified into three GH families (5, 26 and 113), while β-mannosidases belong to GH families 1, 2 and 5 (Sweeney & Xu, 2012). Most of the reported β-mannosidases are members of GH families 1 and 2 (Reddy *et al.*, 2013; Tankrathok *et al.*, 2013). It is noted that only GH family 5 contains both β-mannanases and β-mannosidases. Interestingly, all known β-mannanases and β-mannosidases belong to clan GH-A and share a $(\beta/\alpha)_8$-barrel fold structure with the catalytic acid–base and nucleophile glutamates on β-strands 4 and 7, respectively.

A GH family 5 β-mannosidase from the bacterium *Cellvibrio mixtus* (*Cm*Man5A) has been reported and structurally characterized (Dias *et al.*, 2004). *Cm*Man5A shows high structural similarity to the reported β-mannanases but has different properties. It releases mannose from the nonreducing end of manno-oligosaccharides, indicating that *Cm*Man5A is an exo-acting mannanase or β-mannosidase. Structural studies of *Cm*Man5A indicate that dramatic differences in the lengths of three loops modify the active-centre accessibility and thus modulate the specificity from endo to exo (Dias *et al.*, 2004). Furthermore, the crystal structure of *Cm*Man5A in complex with isofagomine lactam (IFL) indicates that the IFL residue in the -1 subsite adopts the energetically unfavoured $B_{2,5}$ conformation (Vincent *et al.*, 2004). To date, a crystal structure of a GH family 5 β-mannosidase in complex with a substrate is not available, and the precise catalytic and substrate-binding profiles of GH family 5 β-mannosidases are still unknown. Some glycosidases are able to perform transglycosylation via a retaining double-displacement mechanism, in which a carbohydrate hydroxyl group can act as an acceptor molecule rather than water in hydrolysis. Transglycosylation thus leads to the synthesis of new glycosides or oligosaccharides longer than the original substrates. Transglycosylation activity has been observed for β-mannosidases from GH families 1 and 2 (Zhang *et al.*, 2009; Park *et al.*, 2011; Eneyskaya *et al.*, 2009) and enzymes from GH family 5 (Couturier *et al.*, 2013; Dias *et al.*, 2004; Dilokpimol *et al.*, 2011; Katrolia *et al.*, 2013).

Rhizomucor miehei CAU432 is a thermophilic fungus that thrives at an optimum temperature of up to 323 K (Katrolia *et al.*, 2013). In previous studies, we have reported the gene cloning and enzymatic characterization of a β-mannanase (*Rm*Man5A) and an α-galactosidase (*Rm*Gal36) from *R. miehei* (Katrolia *et al.*, 2012, 2013). *Rm*Man5A, with a high alkali tolerance, hydrolyzes locust bean gum and konjac powder, yielding mannobiose, mannotriose and a mixture of various manno-oligosaccharides (Katrolia *et al.*, 2013). The synergistic action of *Rm*Man5A and *Rm*Gal36 releases more reducing sugar (>10%) from guar gum compared with the action of *Rm*Man5A alone (data not shown). Here, we describe the cloning, biochemical properties and several crystal structures of complexes with ligand molecules (mannobiose, mannotriose and mannosyl-fructose) of a novel GH family 5 β-mannosidase (*Rm*Man5B) from *R. miehei*. This is the first report of the crystal structures of a fungal β-mannosidase and a GH family 5 β-mannosidase in complex with manno-oligosaccharides and represents a significant advance in the understanding of β-mannosidases.

2. Materials and methods

2.1. Cloning and expression of a fungal β-mannosidase gene

Recombinant DNA techniques as described by Sambrook & Russell (2001) were employed to perform DNA manipulations. The procedure described by Zhou *et al.* (2013) was used with some modifications to clone the β-mannosidase gene (*RmMan5B*) from *R. miehei* CAU432. The degenerate primers Man5BDF and Man5BDR (Supplementary Table S1[1]) were designed on the basis of the conserved sequences (EEFGMA and GDPPHE) of putative fungal GH family 5 β-mannosidases. The full-length cDNA of *RmMan5B* was obtained using a 5′ and 3′ rapid amplification kit (Clontech, Palo Alto, California, USA). The nucleotide sequence of *RmMan5B* has been submitted to the GenBank database and allocated the accession No. KF539413. For phylogenetic analysis, sequence data were imported from UniProt or the PDB. The sequences were aligned using *MUSCLE* (http://www.ebi.ac.uk/Tools/msa/muscle/) and phylogenetic analysis was performed with the neighbour-joining (NJ) method by *MEGA*4 (http://www.megasoftware.net/mega.html).

To express *RmMan5B*, the coding region of the gene without the signal peptide was amplified from cDNA by PCR using the primers *Rm*Man5BF and *Rm*Man5BR (Supplementary Table S1). The PCR product was digested with *Eco*RI and *Not*I, cloned into the expression vector pET-28a and transformed into *Escherichia coli* BL21 (DE3) cells for protein expression. Additionally, the transformant was confirmed by sequencing to ensure that no mutations had occurred during amplification.

2.2. Purification of the recombinant enzymes

The recombinant GH family 5 β-mannanase (*Rm*Man5A) from *R. miehei* was purified as described previously (Katrolia *et al.*, 2013). The purified *Rm*Man5A was further subjected to a Sephacryl S-100 HR gel-filtration column (1 × 100 cm; GE

[1] Supporting information has been deposited in the IUCr electronic archive (Reference: MV5108).

Life Sciences), eluted with 20 m*M* Tris–HCl buffer pH 8.0 containing 100 m*M* NaCl and concentrated to 20 mg ml^{-1} using Amicon centrifugal filter units (Millipore) for crystallization.

E. coli BL21 cells harbouring the recombinant pET-28a/*RmMan5B* vector were inoculated at 310 K in Luria–Bertani (LB) medium containing kanamycin (50 µg ml^{-1}) with shaking until the optical density OD_{600} reached about 0.6–0.8. Isopropyl β-D-1-thiogalactopyranoside (IPTG) was added to a final concentration of 1 m*M* to induce heterologous expression and the culture was further grown at 303 K overnight. For biochemical assays, the recombinant *Rm*Man5B was purified by nickel(II) affinity chromatography as described previously (Katrolia *et al.*, 2013). The purified *Rm*Man5B was exchanged into 20 m*M* Tris–HCl buffer pH 8.0 containing 100 m*M* NaCl and concentrated to 20 mg ml^{-1} for crystallization. The protein concentration was determined by the method of Lowry *et al.* (1951) using bovine serum albumin (BSA) as the standard. Single-amino-acid substitutions of *Rm*Man5B were performed by an overlap extension PCR-based site-directed mutagenesis technique (Sambrook & Russell, 2001) and were confirmed by DNA sequencing. The primers used for the mutations are given in Supplementary Table S1. The mutant proteins were expressed and purified according to the same methods as used for the wild-type *Rm*Man5B.

2.3. Enzyme assays and biochemical characterization

For determination of the activity of *Rm*Man5B, assay mixtures consisting of 3 m*M* *p*-nitrophenyl β-D-mannopyranoside (*p*NPM) in 50 m*M* sodium citrate pH 5.5 and enzyme solution were incubated at 323 K for 10 min. One unit of enzyme activity was defined as the amount of enzyme that liberated 1 µmol *p*-nitrophenol per minute under the conditions described above. To evaluate the substrate specificity of the enzyme towards various mannooligosaccharides, mannobiose (M2), mannotriose (M3), mannotetrose (M4) and mannopentaose (M5) were used as substrates at 0.1%(*w*/*v*). The release of mannose was determined by high-performance liquid chromatography–evaporative light-scattering detection (HPLC–ELSD). HPLC was performed on a Waters Sugar-D column (4.5 × 250 mm). The sugars were eluted with a mobile phase consisting of 75:25(*v*:*v*) acetonitrile:water at a flow rate of 1.0 ml min^{-1}. The activity towards reduced mannooligosaccharides (M2r–M5r) was tested according to the *p*-hydroxybenzoic acid hydrazide [Abz(OH)ONHNH$_3$] method (Martín-Cuadrado *et al.*, 2008), with a substrate concentration of 0.1%(*w*/*v*). One unit of enzyme activity was defined as the amount of enzyme that liberated 1 µmol mannose per minute under the conditions described above.

2.4. Hydrolysis and transglycosylation properties

Purified *Rm*Man5B was incubated with 1%(*w*/*v*) mannooligosaccharides (M2–M4) at 323 K. To demonstrate whether monosaccharides or disaccharides act as acceptors, *Rm*Man5B (0.01 U ml^{-1}) was incubated with 1% (29 m*M*) mannobiose as a donor and 5% (150–330 m*M*) of one of 18 potential acceptors (L-arabinose, xylose, ribose, glucose, galactose, fructose, glucosamine, *N*-acetylglucosamine, rhamnose, sucrose, lactose, maltose, cellobiose, trehalose, melibiose, chitobiose, laminaribiose and xylobiose) at 323 K for 30 min. Samples were boiled for 5 min to terminate the reactions and the reaction products were analyzed by TLC (Katrolia *et al.*, 2013). Transglycosylation products derived from mannotetraose were analyzed by MALDI–TOF MS. For analysis, the sample was diluted 100-fold prior to mixing with an equal volume of matrix (2,5-dihydroxybenzoic acid, 10 mg ml^{-1} in water). Sample (1 µl) was then spotted onto the MALDI plate and analyzed on an AB SCIEX TOF/TOF 5800 system operated in positive-ion mode.

For structural analysis of mannosyl-fructose, a transglycosylation reaction (10 ml) was performed with *Rm*Man5B (0.01 U ml^{-1}), 1%(*w*/*v*) mannobiose and 10%(*w*/*v*) fructose at 323 K for 30 min. The transglycosylation product was purified on an activated charcoal column (16 × 500 mm) and eluted with a linear gradient of 0–15%(*v*/*v*) ethanol at a flow rate of 1 ml min^{-1}. Purified oligosaccharide (20 mg) was freeze-dried and dissolved in deuterium oxide (500 µl) prior to recording spectra on a Bruker Avance 500 NMR spectrometer. A series of one-dimensional (^{1}H and ^{13}C) and two-dimensional NMR (DQFCOSY, NOSEY, gHSQC and gHMBC, where g stands for gradient-enhanced) spectra were acquired using standard pulse sequences.

2.5. Crystallization and data collection

Crystallization experiments were performed in a 48-well plate using the sitting-drop vapour-diffusion method, equilibrating against 100 µl reservoir solution at 293 K. Crystals of *R. miehei* β-mannanase (*Rm*Man5A) were obtained from a reservoir solution consisting of 80 m*M* sodium acetate buffer pH 4.6, 1.6 *M* ammonium sulfate, 6%(*v*/*v*) glycerol. Native *Rm*Man5B (*Rm*Man5B-native) crystals were obtained from a reservoir solution consisting of 16%(*w*/*v*) PEG 4000, 200 m*M* guanidine hydrochloride in 100 m*M* HEPES buffer pH 7.5. To obtain co-crystals of the E202A mutant (*Rm*Man5B/E202A) in complex with ligands, mannobiose (M2), mannotriose (M3) or mannosyl-fructose (ManFru) were added to the *Rm*Man5B/E202A protein solution to final concentrations of 5, 5 and 10%(*w*/*v*), respectively. The crystals of *Rm*Man5B/E202A–M2 and *Rm*Man5B/E202A–ManFru were obtained under the same conditions as those of *Rm*Man5B-native. The crystals of *Rm*Man5B/E202A–M3 were obtained with a reservoir solution consisting of 20%(*w*/*v*) PEG 4000 in 100 m*M* HEPES pH 7.5. The crystals of *Rm*Man5B/E301A were obtained using the same conditions as those of *Rm*Man5B/E202A–M3. For X-ray diffraction experiments, all crystals were soaked briefly in a cryoprotectant solution [the crystallization solution supplemented with 20%(*v*/*v*) glycerol] and flash-cooled in liquid nitrogen prior to data collection.

X-ray diffraction data for crystals of *Rm*Man5A, *Rm*Man5B, *Rm*Man5B/E202A–M3 and *Rm*Man5B/E301A were collected on beamline NE3A at the Photon Factory, High Energy Accelerator Research Organization (KEK), Tsukuba, Japan. X-ray data for *Rm*Man5B/E202A–M2 and *Rm*Man5B/

Table 1
X-ray data-collection and refinement statistics.

Values in parentheses are for the outer shell.

	*Rm*Man5A	*Rm*Man5B-native	*Rm*Man5B/E202A –M2	*Rm*Man5B/E202A –M3	*Rm*Man5B/E202A –ManFru	*Rm*Man5B/E301A
Data-collection statistics						
Radiation source	NE3A, KEK	NE3A, KEK	3W1A, BSRF	NE3A, KEK	BL17U, SSRF	NE3A, KEK
Wavelength (Å)	0.9794	0.9794	1.0000	1.0000	0.9791	1.0000
Space group	*I*222	$P12_11$	$P12_11$	*C*121	$P12_11$	*C*121
Unit-cell parameters						
a (Å)	86.38	50.65	51.62	131.17	50.81	131.98
b (Å)	89.71	171.99	175.85	76.55	171.93	76.99
c (Å)	111.29	55.14	56.30	54.84	55.16	55.08
β (°)		104.60	104.34	113.36	104.25	113.34
Resolution range (Å)	50.0–2.26 (2.30–2.26)	50–1.28 (1.30–1.28)	50–2.60 (2.64–2.60)	50–2.00 (2.03–2.00)	50–2.40 (2.44–2.40)	50–2.50 (2.54–2.50)
Total No. of reflections	129348	2025731	96945	226283	217682	110754
Unique reflections	18610 (745)	205153 (10741)	28432 (1297)	31831 (1069)	32833 (1229)	16116 (1113)
Multiplicity	7.0 (5.7)	9.9 (7.8)	3.4 (2.7)	7.1 (5.2)	6.6 (5.2)	6.9 (5.6)
Completeness (%)	90.2 (74.0)	87.6 (91.4)	96.8 (88.3)	94.5 (63.1)	91.3 (70.4)	91.5 (55.3)
Mean $I/\sigma(I)$	26.37 (3.24)	54.3 (12.9)	11.9 (2.36)	59.2 (25.0)	32.7 (18.7)	70.2 (46.2)
$R_{\rm merge}$† (%)	5.6 (30.5)	5.2 (25.4)	9.9 (33.0)	4.4 (9.1)	4.6 (7.4)	4.1 (6.1)
B factor from Wilson plot (Å^2)	31.07	9.03	32.80	8.63	18.61	12.68
Refinement and model statistics						
Resolution (Å)	50.0–2.26 (2.32–2.26)	50.0–1.28 (1.31–1.28)	50.0–2.60 (2.67–2.60)	50.0–2.00 (2.05–2.00)	50.0–2.40 (2.46–2.40)	50.0–2.50 (2.56–2.50)
No. of reflections	17561 (1074)	192973 (13963)	26912 (1390)	30235 (1473)	30968 (1746)	15303 (663)
$R_{\rm work}$‡ (%)	22.4 (38.3)	14.8 (36.9)	21.5 (27.0)	15.3 (14.6)	16.6 (17.6)	14.4 (17.7)
$R_{\rm free}$‡ (%)	26.0 (43.6)	17.2 (37.4)	25.9 (32.8)	18.1 (20.2)	20.5 (24.9)	18.2 (31.6)
No. of residues	357	831	831	414	831	414
No. of water molecules	224	958	227	261	454	265
Ligands	—	Tris	M2	M3	ManFru	Tris
R.m.s.d., bond lengths (Å)	0.007	0.007	0.006	0.010	0.007	0.009
R.m.s.d., angles (°)	1.128	1.223	0.940	1.278	1.076	1.252
Mean *B* factor (Å^2)						
Main chain/side chain	37.23/36.97	9.84/10.97	30.49/31.24	7.52/7.99	21.23/23.53	13.47/13.67
Ligands	—	15.03	30.84	21.18	26.50	26.28
Other heteroatoms	51.60	16.30	—	—	—	—
Solvent	41.43	19.93	30.00	13.38	26.92	17.63
MolProbity statistics						
Ramachandran						
Most favoured (%)	94.65	97.90	97.28	98.10	97.74	97.36
Allowed (%)	5.07	2.10	2.72	1.90	2.26	2.64
Outlier (%)	0.28	0.00	0.00	0.00	0.00	0.00
Rotamer outliers (%)	2.39	1.79	1.28	1.12	1.57	1.71
Clashscore (%)	6.75	2.48	0.84	0.91	1.53	2.00
PDB code	4qp0	4lyp	4nrs	4lyq	4nrr	4lyr

† $R_{\rm merge} = \sum_{hkl}\sum_i |I_i(hkl) - \langle I(hkl)\rangle| / \sum_{hkl}\sum_i I_i(hkl)$, where $I_i(hkl)$ is the intensity of observation *i* of reflection *hkl* and $\langle I(hkl)\rangle$ is the weighted average intensity for all observations *i* of reflection *hkl*. ‡ $R_{\rm work} = \sum_{hkl} ||F_{\rm obs}| - |F_{\rm calc}|| / \sum_{hkl} |F_{\rm obs}|$ for reflections in the working set, where $F_{\rm obs}$ and $F_{\rm calc}$ are the observed and calculated structure factors, respectively. $R_{\rm free}$ is calculated analogously for test reflections randomly selected and excluded from the refinement.

E202A–ManFru were collected on the 3W1A beamline at the Beijing Synchrotron Radiation Facility (BSRF) and the BL17U beamline at the Shanghai Synchrotron Radiation Facility (SSRF), People's Republic of China, respectively. All diffraction data were indexed, integrated and scaled using *HKL*-2000 (Otwinowski & Minor, 1997).

2.6. Structure determination and refinement

The structures of *Rm*Man5A and *Rm*Man5B were solved by the molecular-replacement method with *phenix.automr* (Adams *et al.*, 2010) using the *Trichoderma reesei* β-mannanase structure (*Tr*Man5A; PDB entry 1qno, sequence identity 39%; Sabini *et al.*, 2000) and the *Cm*Man5A structure (PDB entry 1uuq, sequence identity 35%; Dias *et al.*, 2004) as search models, respectively. *Phenix.autobuild* (Adams *et al.*, 2010) was used for model rebuilding. The structures were completed with alternating rounds of manual model building with *Coot* (Emsley & Cowtan, 2004) and refinement with *REFMAC*5 (Murshudov *et al.*, 2011). A subset consisting of a randomly selected 5% of reflections was excluded from computational refinement to calculate the $R_{\rm free}$ factor throughout the refinement (Brünger, 1993). The final models were validated by *MolProbity* (Chen *et al.*, 2010). Structural superpositions were calculated by *LSQMAN* (Kleywegt, 1999). Analysis of the protein–ligand interactions was performed in *LigPlus* (Laskowski & Swindells, 2011). Molecular and electron-density illustrations were prepared in *PyMOL* (v.1.3; Schrödinger). The data-collection and refinement statistics for the final refined molecule geometry are listed in Table 1.

To explore the substrate binding of *Rm*Man5A, mannopentaose was modelled into the putative subsites −3 to +2

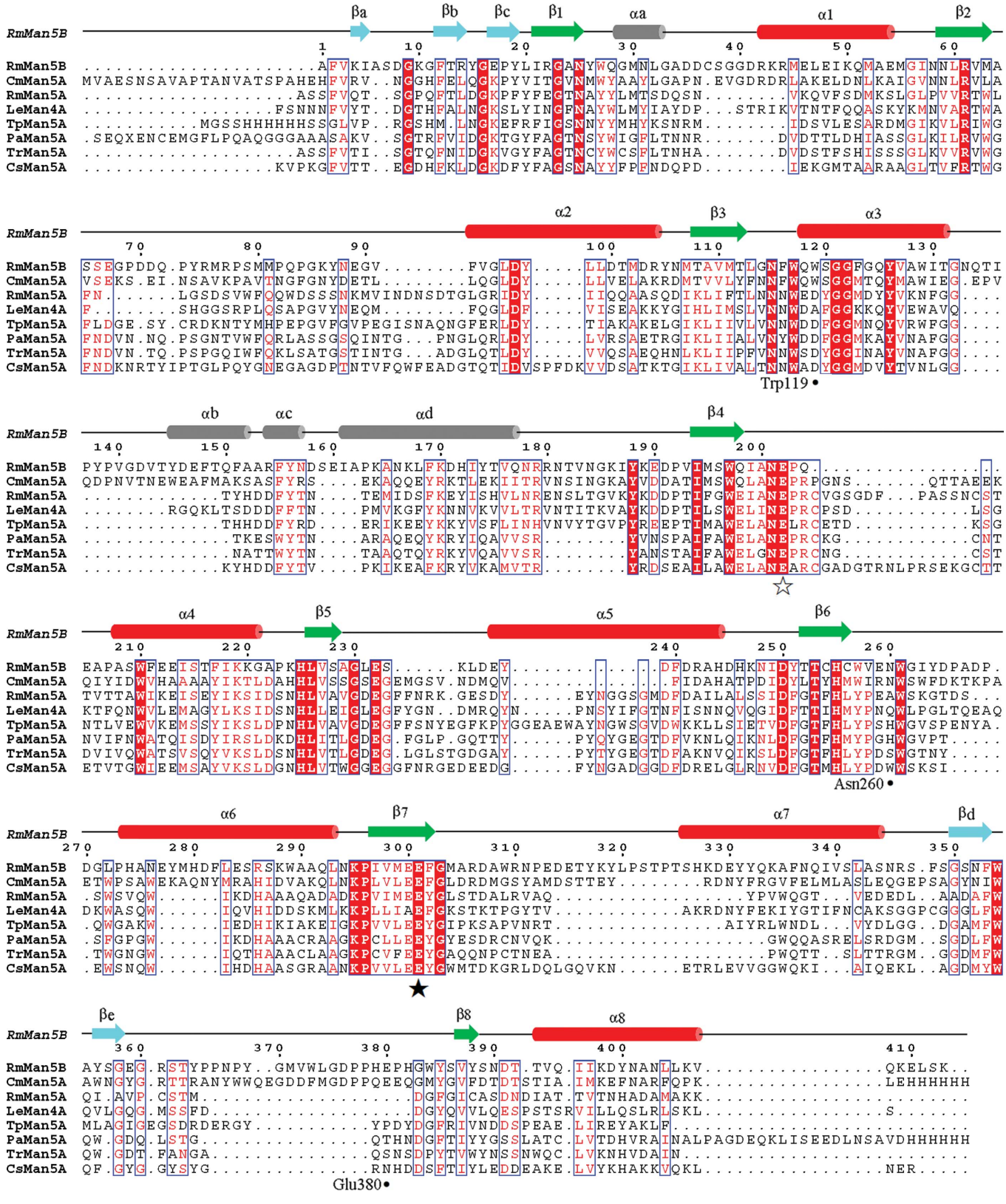

Figure 1
Sequence alignment of *Rm*Man5B with some GH family 5 members. Residues forming the secondary structures of *Rm*Man5B are highlighted above the sequences. Identical residues are shown in white on a red background and conservative residues are shown in red on a white background. The catalytic residues are marked by empty (acid–base) and filled (catalytic nucleophile) stars. The sequences of *Rm*Man5A, *Rm*Man5B, *C. mixtus* β-mannosidase (*Cm*Man5A; PDB entry 1uuq), *L. esculentum* Man4A (*Le*Man4A; PDB entry 1rh9), *T. petrophila* Man5A (*Tp*Man5A; PDB entry 3pz9), *P. anserina* Man5A (*Pa*Man5A; PDB entry 3ziz), *T. reesei* Man5A (*Tr*Man5A; PDB entry 1qno) and *C. sitophila* Man5A (*Cs*Man5A; PDB entry 4awe) were aligned by *MUSCLE* (http://www.ebi.ac.uk/Tools/msa/muscle/) and the figure was generated by *ESPript* (Gouet *et al.*, 2003) with manual modifications.

according to the method described by Bourgault *et al.* (2005), while the *Rm*Man5B/E202A–M3 structure was used to model the −1 mannose residue. The complex model was subjected to energy minimization in the CHARMM force field (Brooks *et al.*, 2009) with the *Discovery Studio* 2.5 package (Accelrys; http://accelrys.com/products/discovery-studio). To visualize the existence of Glu202 in *Rm*Man5B/E202A–M3, a side chain of the Glu202 residue was modelled by superposition with the native *Rm*Man5B structure and the overall structure was optimized by the energy-minimization function of *REFMAC*5.

2.7. PDB accession code

The atomic coordinates and structure factors for the crystal structures of *Rm*Man5A, *Rm*Man5B and its derivatives have been deposited in the Protein Data Bank (PDB; Research Collaboratory for Structural Bioinformatics, Rutgers University, New Brunswick, New Jersey, USA; http://www.pdb.org) under accession codes 4qp0, 4lyp, 4lyq, 4lyr, 4nrs and 4nrr.

3. Results and discussion

3.1. Gene cloning and sequence analysis

A partial β-mannosidase gene (*RmMan5B*) from *R. miehei* was amplified by PCR using degenerate primers. 5′ and 3′ rapid amplification of cDNA ends (RACE) yielded 1143 and 281 bp DNA fragments, respectively. *RmMan5B* contains an open reading frame (ORF) of 1353 bp which encodes a protein of 450 amino-acid residues. The N-terminal region (1–20) was predicted to be a signal peptide using *SignalP* 4.0 (Petersen *et al.*, 2011).

According to a homology search using *PSI-BLAST* (Altschul *et al.*, 1997), the deduced amino-acid sequence of *Rm*Man5B shows 35% identity to the β-mannosidase from the bacterium *C. mixtus* (*Cm*Man5A; PDB entry 1uuq; Dias *et al.*, 2004). However, *Rm*Man5B shares much lower amino-acid sequence identities with other structurally determined GH family 5 β-mannanases, including *Lecopersicon esculentum* Man4A (*Le*Man4A; PDB entry 1rh9; Bourgault *et al.*, 2005), *Thermotoga petrophila* Man5A (*Tp*Man5A; PDB entry 3pz9; Santos *et al.*, 2012), *Podospora anserina* Man5A (*Pa*Man5A; PDB entry 3ziz; Couturier *et al.*, 2013), *Chrysonilia sitophila* Man5A (*Cs*Man5A; PDB entry 4awe; Gonçalves *et al.*, 2012) and *Trichoderma reesei* Man5A (*Tr*Man5A; PDB entry 1qno; Sabini *et al.*, 2000), with identities of 23, 22, 19, 18 and 17%, respectively (Fig. 1). Pairwise comparisons revealed only 19% identity between *Rm*Man5A and *Rm*Man5B. GH family 5 enzymes have been further classified into 51 subfamilies according to the similarity of their amino-acid sequences (Aspeborg *et al.*, 2012). All of these β-mannosidases (*Rm*Man5B and *Cm*Man5A) and β-mannanases belong to GH subfamily 5_7, which consists of archaeal, bacterial and eukaryotic members.

Phylogenetic analysis of the GH subfamily 5_7 member sequences generated a tree in which all 43 sequences were placed into two major clades (Supplementary Fig. S1). Clade A contained 26 sequences and included several known β-mannanases. Clade B contained 17 sequences and consisted of all known GH subfamily 5_7 β-mannosidases. Alignment of the sequences from clade B (data not shown) showed that all of the proteins lacked the tyrosine and tryptophan that play a key role in mannose recognition at the −2 subsite (Bourgault *et al.*, 2005; Gonçalves *et al.*, 2012). However, the enzymes have extended loops between strand β8 and helix α8 that modify the active-centre accessibility (Dias *et al.*, 2004) and three residues (Trp119, Asn260 and Glu380; see below) which are probably important for the exo-activity of GH family 5 β-mannosidases. We therefore predict that the clade B enzymes should display β-mannosidase activity. Recently, a new GH subfamily 5_19 β-mannosidase from *Thermotoga thermarum* (*Tth*Man5) has been functionally characterized (Shi *et al.*, 2013). GH subfamily 5_19 contains only archaeal sequences, which are distinct from those of GH subfamily 5_7 enzymes (Aspeborg *et al.*, 2012). As the crystal structure of *Tth*Man5 is not available, the molecular determinants which confer the β-mannosidase activity are unknown.

Table 2
Substrate specificity of *Rm*Man5B.

Substrate	Specific activity† (U mg^{-1})	Relative activity (%)
*p*NP-β-mannopyranose	1.93 ± 0.03	1.74
Mannobiose	66.5 ± 4.9	60.0
Mannotriose	110.9 ± 4.4	100
Mannotetraose	99.3 ± 8.2	89.5
Mannopentaose	101.7 ± 6.5	91.7
Mannosyl-fructose	23.3 ± 1.0	21.0
Reduced mannobiose	NA‡	0
Reduced mannotriose	46.2 ± 1.0	41.7
Reduced mannotetraose	108.5 ± 2.1	97.8
Reduced mannopentaose	111.2 ± 8.3	100.3

† Enzymatic reactions were carried out for 10 min at 50°C in 50 m*M* citrate buffer pH 5.5 as described in the text. ‡ No activity was detected.

3.2. Biochemical properties of *Rm*Man5B

RmMan5B was expressed in *E. coli* BL21 cells as a soluble intracellular enzyme and was purified by Ni^{2+}-affinity chromatography with 3.7-fold purification and an overall yield of 57% (data not shown). The purified enzyme migrated on SDS–PAGE as a single homogeneous band of 52 kDa, matching the molecular mass (51 259 Da) calculated from the deduced amino-acid sequence (Supplementary Fig. S2). The enzyme showed a specific activity of 66.5 U mg^{-1} using mannobiose as a substrate (Table 2), which is comparable to those reported for other β-mannosidases (Zhang *et al.*, 2009; Shi *et al.*, 2013). *Rm*Man5B hydrolysed mannotriose (110.9 U mg^{-1}) approximately two times faster than mannobiose, whereas the activities of the enzyme towards mannotetraose (99.3 U mg^{-1}) and mannopentaose (101.7 U mg^{-1}) were similar to that towards mannotriose (Table 2). These data indicated that *Rm*Man5B has one glycone (−1) and two aglycone (+1 and +2) subsites that can accommodate β-1,4-linked mannose residues. However, *Rm*Man5B exhibited a much higher activity towards manno-oligosaccharides than *p*NPM (1.93 U mg^{-1}), although the *p*NP residue is normally a better leaving group. Additionally, *Rm*Man5B showed a

Table 3
Specific activity of wild-type and mutants of *Rm*Man5B.

*Rm*Man5B	Substrate	Specific activity† (U mg^{-1})	Relative activity‡ (%)
Wild type	*p*NP-*β*-mannopyranose	1.93 ± 0.03	100
Trp119Ala	*p*NP-*β*-mannopyranose	NA§	0
Asn260Ala	*p*NP-*β*-mannopyranose	0.30 ± 0.04	15.5
Asn260Ser	*p*NP-*β*-mannopyranose	0.24 ± 0.04	12.4
Asn260Trp	*p*NP-*β*-mannopyranose	0.13 ± 0.02	6.73
His379Gln	*p*NP-*β*-mannopyranose	1.74 ± 0.08	90.2
Glu380Ala	*p*NP-*β*-mannopyranose	NA	0
Wild type	Reduced mannotetraose	108.5 ± 2.1	100
Trp119Ala	Reduced mannotetraose	9.09 ± 0.06	8.38
Asn260Ala	Reduced mannotetraose	0.22 ± 0.01	0.20
Asn260Ser	Reduced mannotetraose	6.09 ± 0.03	5.61
Asn260Trp	Reduced mannotetraose	4.71 ± 0.47	4.34
His379Gln	Reduced mannotetraose	57.5 ± 5.30	53.0
Glu380Ala	Reduced mannotetraose	NA	0

† Enzymatic reactions were carried out for 10 min at 50°C in 50 m*M* citrate buffer pH 5.5 as described in the text. ‡ Activity is represented as a percentage of that found for the wild-type protein. § No activity was detected.

specific activity of 23.3 U mg^{-1} for mannosyl-fructose (Table 2). To determine the activity of *Rm*Man5B towards manno-oligosaccharides more conveniently, reduced mannooligosaccharides were used as substrates. *Rm*Man5B hydrolysed M3r (46.2 U mg^{-1}), M4r (108.5 U mg^{-1}) and M5r (111.2 U mg^{-1}), but did not exhibit any activity towards M2r (Table 3). The hydrolysis products of reduced mannotriose (M3r) by *Rm*Man5B are mannose and mannobiose, confirming that *Rm*Man5B releases mannose from the non-reducing end of mannooligosaccharides (Supplementary Fig. S3).

*Rm*Man5B showed transglycosylation activities towards manno-oligosaccharides even at relatively low substrate concentrations (0.1%). At high concentrations (1%) of mannobiose and mannotriose the enzyme showed strong transglycosylation activity during the initial period (Supplementary Fig. S4). *Rm*Man5B catalysed the transglycosylation of M2, resulting in M3 and M4, while M4–M7 were obtained using M3 as substrate (Fig. 2*a*). There was even a small quantity of M11 detected by MALDI-TOF MS when M4 was used as the substrate (Fig. 2*c*, Supplementary Fig. S4). Moreover, the enzyme had a transglycosylation activity which transferred mannosyl residues to fructose, galactose, sucrose and laminaribiose among 18 tested acceptors, resulting in novel hetero-mannooligosaccharides (Fig. 2*b* and Supplementary Fig. S5). To our surprise, fructose was the best acceptor for transglycosylation. The structure of the transglycosylation product (mannosyl-fructose) was assigned by two-dimensional NMR (Supplementary Table S2). The mannosyl-fructose (*β*-D-mannopyranosyl-(1→4)-D-fructose; Supplementary Fig. S6) showed a *β*-1,4 linkage between mannosyl and the fructose acceptor, as shown by the downfield shift of C-4 in the fructose residue. The chemical shifts of the mannosyl residue fit the calculated data for the *β*-mannosyl residue at the nonreducing end of mannobiose well (http://www.casper.organ.su.se/casper/). The ^{13}C NMR spectrum of mannosyl-fructose in D_2O displayed three sets of signals, indicating an equilibrium mixture of isomers: *β*-D-mannopyranosyl-(1→4)-*β*-D-fructopyranose (1A), *β*-D-mannopyranosyl-(1→4)-*β*-

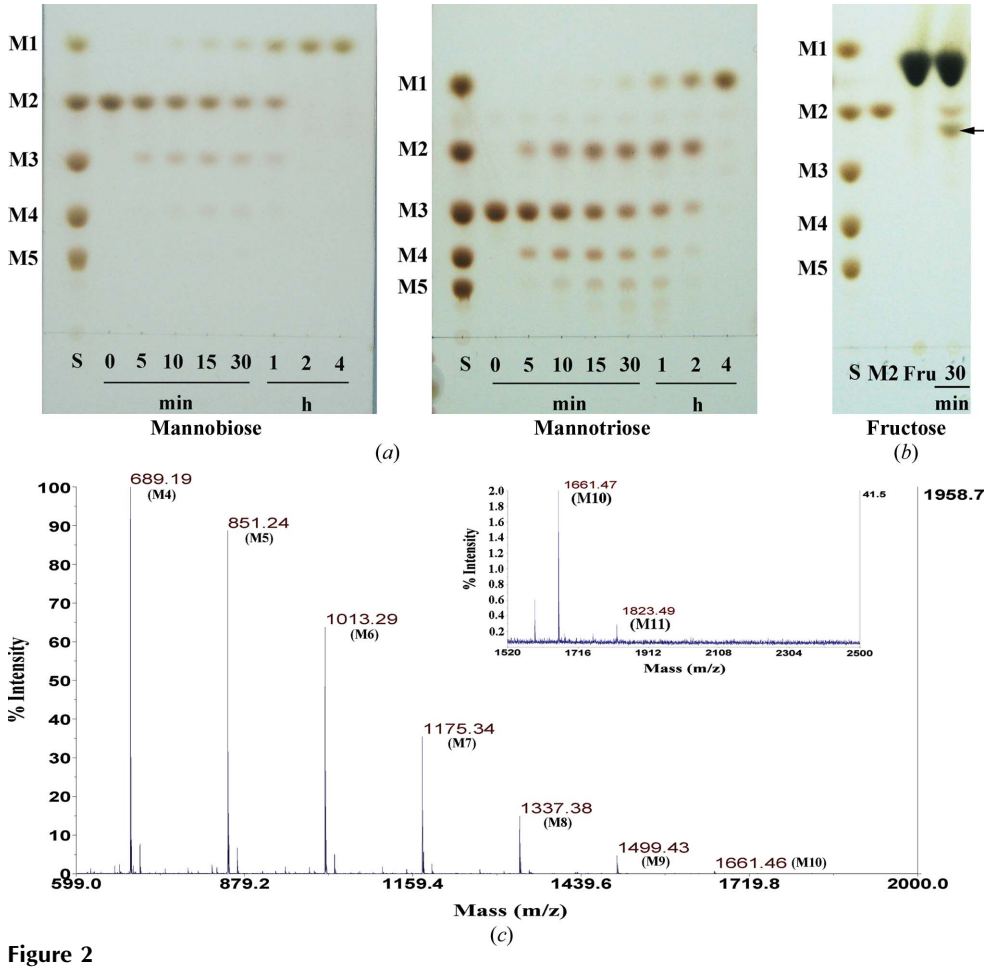

Figure 2
TLC and MALDI-MS analysis of the hydrolysis products of *Rm*Man5B. (*a*) Hydrolysis of mannobiose or mannotriose by *Rm*Man5B. Enzyme (0.01 U ml^{-1}) was incubated with 1% mannobiose or 1%(*w*/*v*) mannotriose in 50 m*M* sodium citrate buffer pH 5.5 at 323 K for 4 h. Incubation times (h or min) are indicated. Lane S, manno-oligosaccharides consisting of mannose (M1), mannobiose (M2), mannotriose (M3), mannotetraose (M4) and mannopentaose (M5). (*b*) Transglycosylation of fructose [5%(*w*/*v*)] using *Rm*Man5B (0.01 U ml^{-1}) incubated with mannobiose [1%(*w*/*v*)] for 30 min. The transglycosylation products spotted on the TLC are marked. (*c*) MALDI-TOF MS spectrum for mannotetraose [1%(*w*/*v*)] taken from a reaction mixture containing 0.01 U ml^{-1} enzyme for 30 min. The peaks in the spectra correspond to the monoisotopic masses of sodium adducts $[M + Na]^+$ of the manno-oligosaccharides.

D-fructofuranose (1B) and β-D-mannopyranosyl-(1→4)-α-D-fructofuranose (1C) (Supplementary Fig. S7) because of the mutarotational equilibrium of the fructose residue between the pyranose and furanose forms (Mayer *et al.*, 2004). The ^{1}H NMR spectrum confirmed the presence of three isomers, 1A, 1B and 1C, in a ratio of ∼60:30:10.

3.3. Overall structures of *Rm*Man5A and *Rm*Man5B

*Rm*Man5A shares amino-acid sequence identities of less than 40% with other structurally determined β-mannanases such as *Cs*Man5A (39% identity), *Tr*Man5A (39%), *Pa*Man5A (38%), *Tp*Man5A (37%) and *Le*Man4A (36%) (Bourgault *et al.*, 2005; Couturier *et al.*, 2013; Gonçalves *et al.*, 2012; Sabini *et al.*, 2000; Santos *et al.*, 2012). The crystal structure of *Rm*Man5A was solved in its free form at 2.3 Å resolution. The overall structure of *Rm*Man5A exhibits a classical $(\beta/\alpha)_8$-TIM barrel fold as expected for enzymes belonging to GH family 5 (Fig. 3*a*). Each monomer of *Rm*Man5A consists of nine α-helices and 12 β-strands. The protein features a roughly V-shaped groove by structural homology with other GH5 members, corresponding to the catalytic groove in which the catalytic acid–base and nucleophile (Glu175 and Glu293) are located (Fig. 3*a* and Supplementary Fig. S8). *Rm*Man5A contains two disulfide bonds: Cys197–Cys209 (at the end of strand β4 and at the beginning of helix α4, respectively) and Cys349–Cys358 (at the end of strand β8 and at the beginning of helix α8, respectively). The number of disulfide bonds in *Rm*Man5A is higher than that in *Tp*Man5A (no disulfide bonds), *Cs*Man5A (one disulfide bond) and *Le*Man4A (one disulfide bond), but lower than that in *Tp*Man5A (three disulfide bonds) and *Tr*Man5A (four disulfide bonds) (Bourgault *et al.*, 2005; Couturier *et al.*, 2013; Gonçalves *et al.*, 2012; Sabini *et al.*, 2000; Santos *et al.*, 2012).

The structure of *Rm*Man5B-native was determined at 1.28 Å resolution. *Rm*Man5B also displays the $(\beta/\alpha)_8$-barrel architecture (Fig. 3*b*). Each monomer of *Rm*Man5B consists of 12 α-helices and 13 β-strands. Unlike *Rm*Man5A, the active site of *Rm*Man5B forms a 15–20 Å deep slot-like pocket which is located on connecting loops at the C-terminal end of the

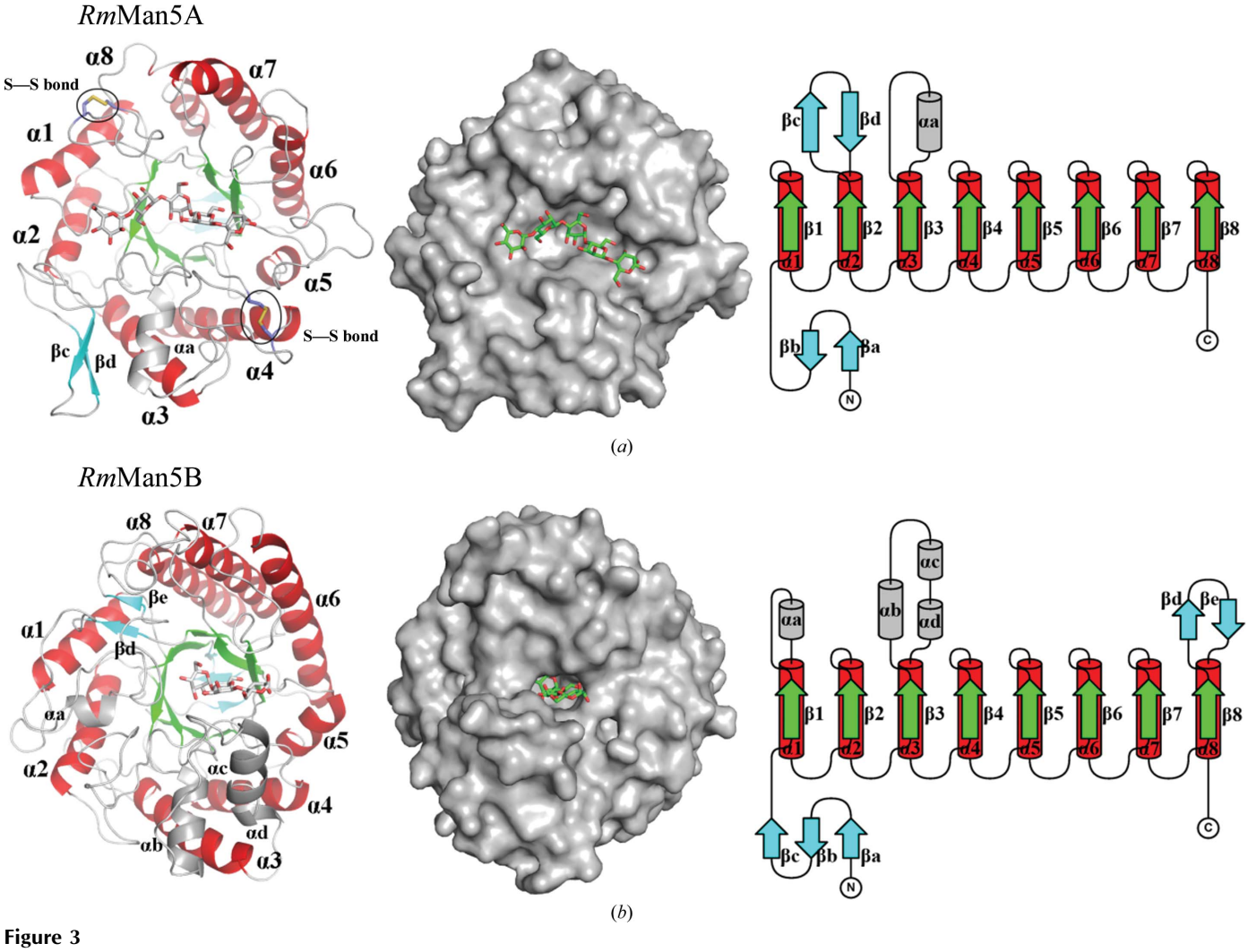

Figure 3
The overall folds of *Rm*Man5A and *Rm*Man5B. Ribbon diagrams, molecular surfaces and topologies of the secondary-structure elements of (*a*) *Rm*Man5A and (*b*) *Rm*Man5B are shown. Mannano-oligosaccharides are shown in stick representation. All figures were generated by *PyMOL* v.1.3 (http://www.pymol.org; Schrödinger) and *TopDraw* (Bond, 2003).

β-sheets of the $(\beta/\alpha)_8$-barrel. *Rm*Man5B has no intramolecular disulfide bond. However, there is one disulfide bond between two monomers in the asymmetric unit (Supplementary Fig. S9). The native molecular mass of *Rm*Man5B-native as determined by gel filtration was 48 kDa, indicating that the enzyme is a monomer in solution (data not shown). In addition, there are no specific interactions that can result in the formation of the dimeric structures revealed by the *Protein Interfaces, Surfaces and Assemblies* (*PISA*) server (Krissinel & Henrick, 2007). Two monomers might interact to form the disulfide bond through crystallographic packing.

In the structure of *Rm*Man5B-native one Tris molecule and one guanidine (GAI) molecule were found to bind at the active site. Meanwhile, one Tris molecule was also observed to bind at the active site of *Rm*Man5B/E301A (Supplementary Fig. S10). Although the Tris molecules of the two crystal structures are located at similar positions, they are bound in different orientations. In previous reports, Tris served as an inhibitor and has been observed in the structures of some β-mannanases and glycosidases (Sabini *et al.*, 2000; Gonçalves *et al.*, 2012). Tris significantly inhibits the activity of *Rm*Man5B (Supplementary Fig. S11*a*; 35% activity at 20 m*M*). However,

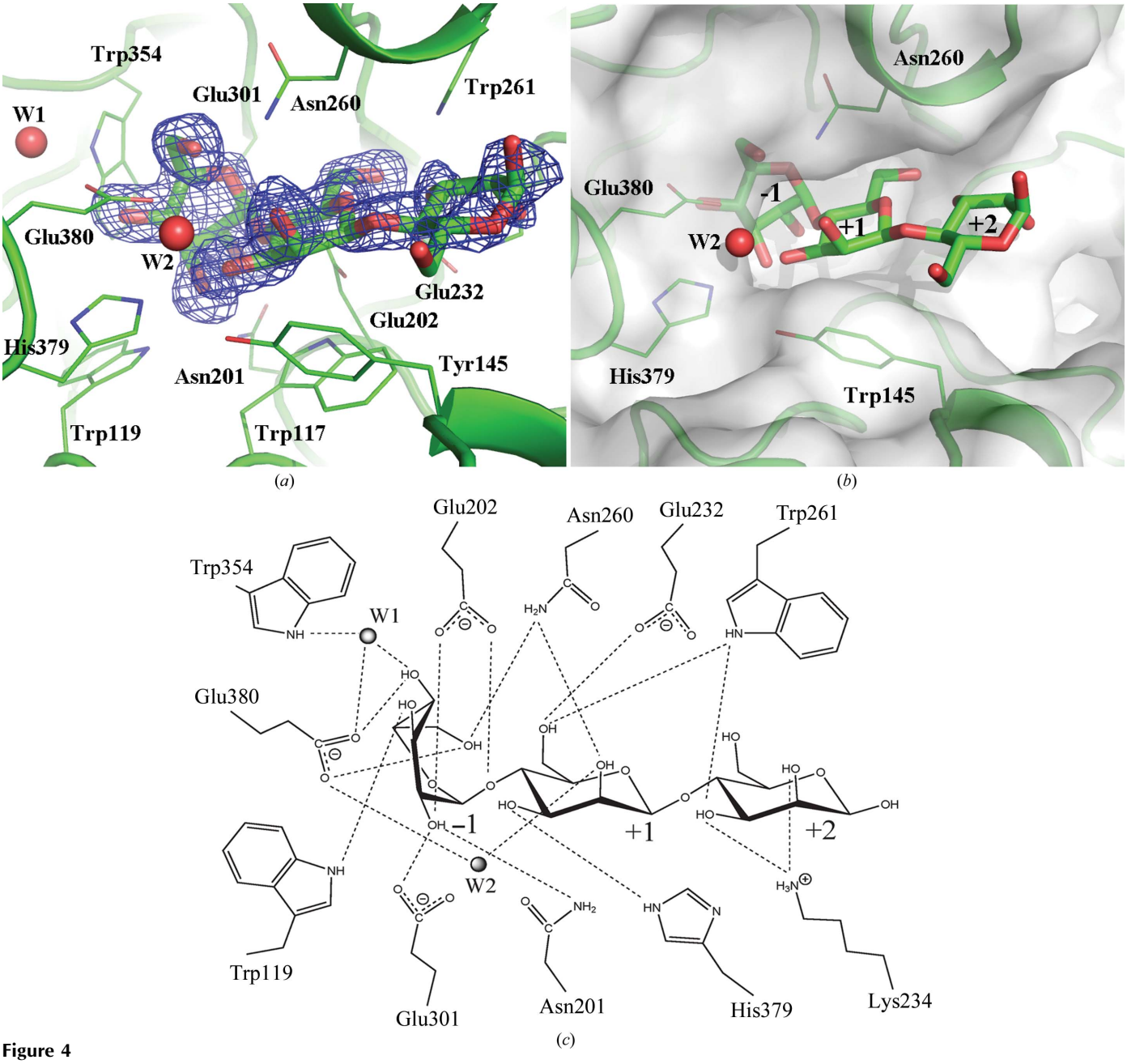

Figure 4
Interactions of the substrate in the active site of *Rm*Man5B/E202A–M3. (*a*) The crystal structure of *Rm*Man5B/E202A in complex with mannotriose. The σ_A-weighted $mF_o - DF_c$ OMIT electron-density map contoured at 3.0σ for mannotriose is shown as a blue mesh. (*b*) Surface representation of the *Rm*Man5B catalytic gorge. The extended loop between strand β8 and helix α8 (His379 and Glu380) modified the active-centre accessibility. (*c*) Schematic drawing of hydrogen-bonding interactions between mannotriose and residues at subsites −1 to +2. All figures were generated by *PyMOL* v.1.3 and *ChemDraw* (CambridgeSoft, Cambridge, Massachusetts, USA).

no significant inhibition is observed by guanidine hydrochloride even at 200 m*M* (Supplementary Fig. S11*b*; 90% activity).

3.4. Crystal structures of *Rm*Man5B complexes

The structure of *Rm*Man5B/E202A in complex with mannotriose (*Rm*Man5B/E202A–M3) was determined at 2.0 Å resolution. The interactions between the substrate molecule and *Rm*Man5B are shown in Fig. 4. Three mannose residues (in the −1 to +2 subsites) are well defined in the electron-density maps, except for C-6 and the corresponding hydroxyl group of the subsite +2 mannose. The average temperature factors of mannotriose corresponding to positions −1, +1 and +2 are 15.2, 20.6 and 30.0 Å^2, respectively. We also obtained a crystal of *Rm*Man5B/E202A in complex with mannobiose (*Rm*Man5B/E202A–M2), which was solved at 2.6 Å resolution (Supplementary Fig. S12). Superposition of *Rm*Man5B/E202A–M3 with *Rm*Man5B-native showed that nearly all of the residues in the cleft were in the same positions; only the side chain of Lys234 displayed a significant variation (Supplementary Fig. S13). The Lys234 residues in *Rm*Man5B and *Rm*Man5B/E202A–M3 have similar χ_1 (∼75°) and χ_2 (∼178°) angles but different χ_3 angles (∼165° and ∼80°, respectively).

In the *Rm*Man5B/E202A–M3 structure the mannose residue of the −1 subsite is located at the bottom of the active-site pocket (Fig. 4). Trp354 stacks against the mannose to form the hydrophobic sugar-binding platform. Eight tight hydrogen-bonded contacts to the hydroxyl groups on C-2, C-3, C-4 and C-6 lock the nonreducing terminal sugar into place and are consistent with the exo-specificity of the enzyme. At the +1 subsite, Trp117 forms the hydrophobic sugar-binding platform. The mannose residue makes a network of five hydrogen bonds to Glu232, Asn260, Trp261 and His379 and one water molecule. In previous reports (Dias *et al.*, 2004), the +1 subsite of *Cm*Man5A exhibits a strong preference for mannose, although it will interact weakly with glucose. *Rm*Man5B has an asparagine residue, Asn260, positioned to interact with O-2 of the +1 mannose, suggesting that *Rm*Man5B cannot or can only weakly bind a glucosyl group at the +1 subsite. At the +2 subsite a wider cleft was observed. The mannose residue only makes a network of three hydrogen bonds with two residues (Lys234 and Trp261). The wide cleft combined with a flexible C-6 hydroxyl suggested that *Rm*Man5B can accommodate a galactose side chain in the +2 subsite. This structural evidence also agrees with the enzymatic properties of *Cm*Man5A (Dias *et al.*, 2004).

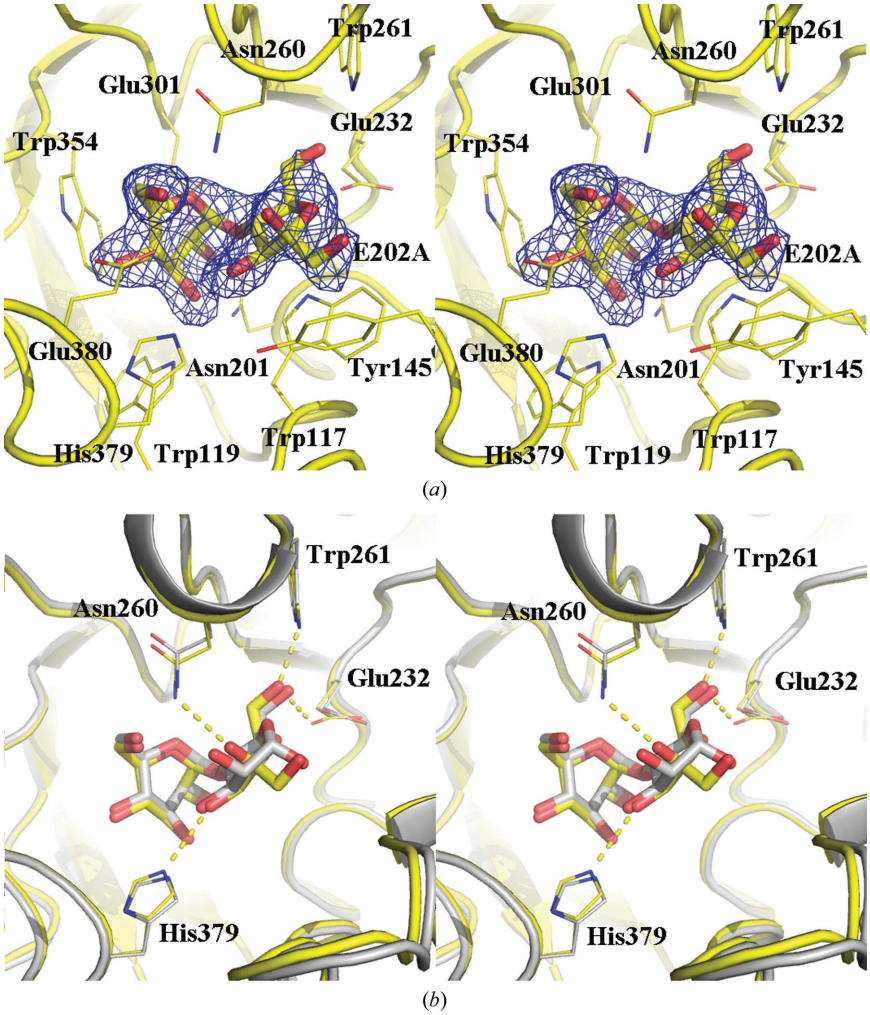

Figure 5
Stereoview of the active site of *Rm*Man5B/E202A–ManFru. (*a*) The crystal structure of *Rm*Man5B/E202A in complex with mannosyl-fructose. The σ_A-weighted $mF_o - DF_c$ OMIT electron-density map contoured at 3.0σ for mannosyl-fructose is shown as a blue mesh. (*b*) Structural superposition of *Rm*Man5B/E202A–M2 and *Rm*Man5B/E202A–ManFru. The side chains of the protein involved in hydrogen bonds to the +1 mannose and fructose residue are shown in stick representation and hydrogen-bond interactions are shown as dotted lines. All figures were generated by *PyMOL* v.1.3.

In the *Rm*Man5B/E202A–M3 structure the −1 mannose residue displays a $^1S_5$ skew-boat conformer and the +1 and +2 mannose residues adopt the energetically favourable $^4C_1$ configuration. In β-mannosidases (GH families 1 and 2) and β-mannanases (GH families 5 and 26), the sugar residue occupying the −1 subsite adopts the $^1S_5$ configuration prior to hydrolysis (Ducros *et al.*, 2002; Bourgault *et al.*, 2005; Tailford *et al.*, 2008; Tankrathok *et al.*, 2013). In the crystal structure of *Cm*Man5A–IFL, IFL adopts the $B_{2,5}$ conformation (Vincent *et al.*, 2004). The extensive literature supports the proposal that the hydrolysis of GH family 5 β-mannosidases follows a $^1S_5 \rightarrow B_{2,5} \rightarrow {}^OS_2$ itinerary from the Michaelis complex to the transition state to the covalent enzyme–substrate intermediate (Bourgault *et al.*, 2005; Vincent *et al.*, 2004). This itinerary

allows the C-2 hydroxyl to remain pseudo-equatorial over the course of the formation of the enzyme–sugar intermediate (Tailford *et al.*, 2008).

To provide evidence for the interactions between *Rm*Man5B and mannosyl-fructose, the transglycosylation product was co-crystallized with *Rm*Man5B (*Rm*Man5B/E202A–ManFru; Fig. 5*a*). The resolution of this complex was limited to 2.4 Å, which resulted in a calculated σ_A-weighted $mF_o - DF_c$ OMIT electron-density map in which the mannose residue could be placed unambiguously. The density clearly showed the presence of D-fructofuranose in the β-anomeric configuration. The average temperature factors of the sugar residues at subsites −1 and +1 are 22.2 and 28.6 Å^2, respectively. Analysis of the ^{1}H NMR spectrum confirmed the presence of three isomers in the aqueous solution of mannosyl-fructose: β-D-mannopyranosyl-β-D-fructopyranose (∼60%), β-D-mannopyranosyl-β-D-fructofuranose (∼30%) and β-D-mannopyranosyl-α-D-fructofuranose (∼10%; Supplementary Fig. S6). However, in the *Rm*Man5B/E202A–ManFru structure the mannosyl-fructose displays the β-D-mannopyranosyl-β-D-fructofuranose configuration. Superposition of the mannosyl-fructose complex and the *Rm*Man5B/E202A–M2 structure showed that the D-fructofuranose was essentially in the same position as the +1

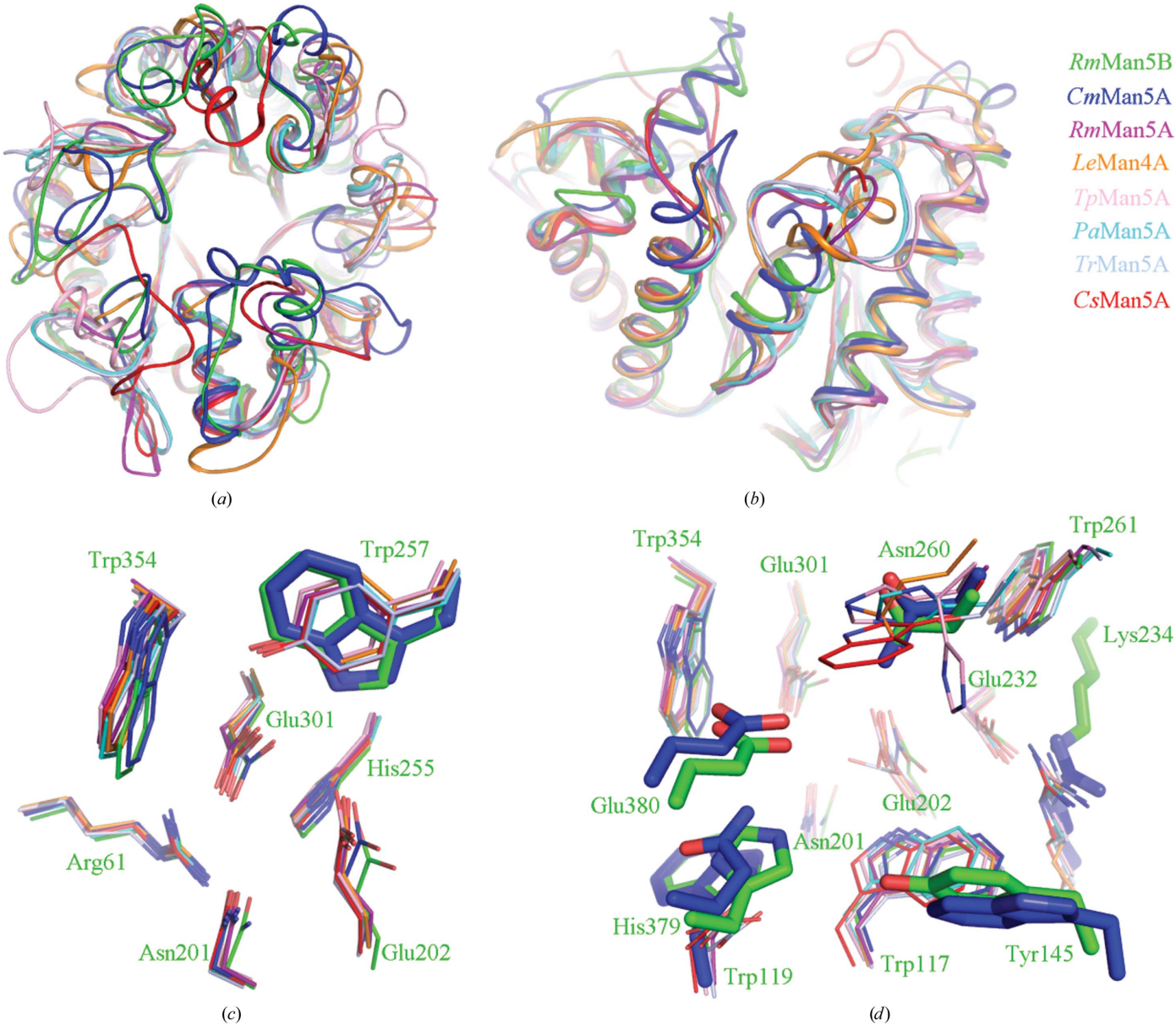

Figure 6
Comparison of *Rm*Man5B with other GH family 5 β-mannanases and β-mannosidase. (*a*) Side view and (*b*) top view of the superimposition of *Rm*Man5B and the enzymes. Details of (*c*) the highly conserved major residues in GH family 5 and (*d*) the residues forming the subsites are shown. The different amino-acid residues are highlighted in stick representation. The C atoms of the residues are coloured according to the enzyme: *Rm*Man5B in green, *Cm*Man5A in blue, *Rm*Man5A in purple, *Le*Man4A in orange, *Tp*Man5A in pink, *Pa*Man5A in cyan, *Tp*Man5A in light blue and *Cs*Man5A in red. All figures were generated by *PyMOL* v.1.3.

mannose residue in the *Rm*Man5B/E202A–M2 structure (Fig. 5*b*). The structural evidence in this study explains why fructose is an effective transglycosylation acceptor.

3.5. Comparison of the active sites of GH family 5 members

*Rm*Man5B shows the highest structural similarity to the *C. mixtus* β-mannosidase (*Cm*Man5A; Figs. 6*a* and 6*b*; Supplementary Fig. S14). Superimposition of *Rm*Man5B with other β-mannanases shows that the $(\beta/\alpha)_8$-barrel core structures superimpose particularly well, while the interconnecting loops vary considerably. As suggested previously, the extended loops of GH family 5 β-mannosidases modify the active-centre accessibility and modulate the specificity from endo to exo (Dias *et al.*, 2004). The *C. sitophila* β-mannanase (*Cs*Man5A) also has several extended loops at the top of the β-barrel; however, these loops show a different arrangement compared with those in *Rm*Man5B. The extended loops of the *Cs*Man5A structure have been suggested to contribute to the enclosure of the cleft (Gonçalves *et al.*, 2012).

In the −1 and +1 subsites, seven of the eight residues that are highly conserved in GH family 5 enzyme structures (Hilge *et al.*, 1998) are found in the β-mannanases and six are found in the β-mannosidases (Fig. 6*c*; Arg61, Asn201, Glu202, His255, Glu301 and Trp354; the conserved tyrosine in the β-mannanases aligns with Trp257 in *Rm*Man5B). Trp354 forms the hydrophobic sugar-binding platform at the −1 subsite. Asn201 plays an important role in stabilizing the transition state by making a hydrogen bond to the O-2 of the sugar in the −1 subsite. The catalytic acid–base Glu202 forms a hydrogen bond to His255 and the conformation of the catalytic nucleophile Glu301 is stabilized through hydrogen bonds to Arg61 and Trp257.

In *Rm*Man5B, the extended loop between strand β8 and helix α8 (residues 354–392) forms a 'double' steric barrier to 'block' the substrate-binding cleft at the end of the −1 subsite. The complex structures and structural comparisons showed that three additional residues (Trp119, Asn260 and Glu380) might be important in GH family 5 β-mannosidases (Fig. 6*d*; Supplementary Fig. S14). Trp119 (which aligns with an aspartic acid in the β-mannanases) is involved in polar contacts with the O-3 of the mannose residue located at the −1 subsite (Fig. 4*c*). Asn260 interacts with O-6 of the −1 mannose residue and O-2 of the +1 mannose residue, and Glu380 lies at the extreme end of the tunnel and interacts with O-4 and O-6 of the nonreducing −1 mannosyl residue. W119A, D260A, D260S, D260W and E380A mutations decreased the activity (Table 3), clearly indicating that these three residues, which are involved in hydrogen bonds contacting the −1 mannose residue, are essential for catalytic activity. Additionally, Tyr154 in the extended long loop (residues 133–150) creates a steric block at one side of the substrate cleft of the +1 and +2 subsites.

Usually β-mannanases recognize at least four mannose units, although some β-mannanases are also able to hydrolyse mannotriose (Sabini *et al.*, 2000). β-Mannanases and the β-mannosidase are extremely similar in the +1 and +2 subsites, suggesting that the binding energy from the +1 and +2 subsites of *Rm*Man5B is also required for efficient catalysis. However, *Rm*Man5B has more interactions at the −1 subsite. *Rm*Man5B hydrolyses mannobiose and *p*NPM, highlighting the pivotal role of the −1 binding site in the β-mannosidase.

*Rm*Man5B has 35% identity but shows high structural similarity to *Cm*Man5A. Large differences in the enzymatic properties are also noted: *Rm*Man5B hydrolyses mannotriose two times faster than mannobiose, while *Cm*Man5A hydrolyses mannobiose very slowly and has a high level of affinity for the third mannanosyl residue of mannotriose at the +2 subsite. The hydrolysis activity of *Rm*Man5B is ∼100-fold and ∼30-fold higher than that of *Cm*Man5A towards *p*NPM and mannobiose, respectively. In addition, *Cm*Man5A cannot generate larger products when mannobiose is used as the substrate: it might be that hydrolysis is much faster than transglycosylation (Dias *et al.*, 2004). However, these different properties cannot be entirely explained by the differences between the two structures. The one exception is His379 (which aligns with Gln403 in *Cm*Man5A) located in the loop between β8 and α8, which interacts with the hydroxyl group at C-3 of the mannose residue in the +1 subsite. A H379Q mutation results in a decrease in activity towards M4r (53% activity) and *p*NPM (90% activity), suggesting that this is not the main reason for the different catalytic performance of these two enzymes (Table 3). Another important residue is Lys234 (which is located in the β5 and α5 loop in *Rm*Man5B), which has the same function as the arginine residue in *Cm*Man5A (Arg217, located in the β4 and α4 loop) and the β-mannanases. The equivalent residue to *Tr*Man5A has been shown to play a significant role in the transglycosylation ability of *Tr*Man5A (Rosengren *et al.*, 2012; Couturier *et al.*, 2013). The arginine residue might interact with the +2 mannose residue more strongly than the flexible lysine residue; hence *Cm*Man5A derives more of its catalytic power from the +2 subsite.

The relatively high transglycosylation ability of *Rm*Man5B might be interpreted as being owing to stabilizing interactions within the acceptor subsite: the interactions that stabilize the transition state are in both the −1 and +1 (in some cases the −1, +1 and +2) subsites for glycosylation and transglycosylation, but are only located in the −1 subsite for hydrolysis (Street *et al.*, 1992; Teze *et al.*, 2014). Furthermore, site-directed mutagenesis showed that the well conserved residues around the −1 active site of the GH family 1 *Thermus thermophilus* β-glycosidase (*Tt*β-gly) are relevant targets for obtaining very efficient mutants for transglycosylation reactions. These mutants have almost lost their hydrolytic activity while retaining significant transglycosylation activity (Teze *et al.*, 2014).

4. Conclusions

GH family 5 β-mannosidases show high structural similarity to the β-mannanases from this family, but have different properties (Dias *et al.*, 2004). In this study, a fungal GH family 5 β-mannosidase from *R. miehei* (*Rm*Man5B) was functionally

and structurally characterized. The results presented here suggest that evolution has modified the loop regions surrounding the active-centre cleft and varied several critical residues to change a β-mannanase into a β-mannosidase. These modifications have increased the enzyme–substrate interactions at the -1 subsite. Additionally, the +1 and +2 subsites are similar in both β-mannanases and β-mannosidases and are required for efficient catalysis of *Rm*Man5B. Therefore, the β-mannosidase shows a strong transglycosylation activity. Furthermore, the structure in complex with mannosylfructose shows that the interactions between the β-mannosidase and D-fructofuranose are similar to those of mannobiose. This structural evidence explains why fructose is an effective transglycosylation acceptor.

This work was supported in part by the National Science Fund for Distinguished Young Scholars (No. 31325021), the National Natural Science Foundation of China (No. 31272475), the National High Technology Research and Development Program of China (863 Program, No. 2012AA021505) and the German fellowship programme for S&T awardees. We are grateful to the staff of SSRF, BSRF and KEK for their assistance in X-ray data collection.

References

Adams, P. D. *et al.* (2010). *Acta Cryst.* D**66**, 213–221.
Altschul, S. F., Madden, T. L., Schäffer, A. A., Zhang, J., Zhang, Z., Miller, W. & Lipman, D. J. (1997). *Nucleic Acids Res.* **25**, 3389–3402.
Aspeborg, H., Coutinho, P. M., Wang, Y., Brumer, H. III & Henrissat, B. (2012). *BMC Evol. Biol.* **12**, 186.
Bond, C. S. (2003). *Bioinformatics*, **19**, 311–312.
Bourgault, R., Oakley, A. J., Bewley, J. D. & Wilce, M. C. J. (2005). *Protein Sci.* **14**, 1233–1241.
Brooks, B. R. *et al.* (2009). *J. Comput. Chem.* **30**, 1545–1614.
Brünger, A. T. (1993). *Acta Cryst.* D**49**, 24–36.
Chen, V. B., Arendall, W. B., Headd, J. J., Keedy, D. A., Immormino, R. M., Kapral, G. J., Murray, L. W., Richardson, J. S. & Richardson, D. C. (2010). *Acta Cryst.* D**66**, 12–21.
Couturier, M., Roussel, A., Rosengren, A., Leone, P., Stålbrand, H. & Berrin, J. G. (2013). *J. Biol. Chem.* **288**, 14624–14635.
Dhawan, S. & Kaur, J. (2007). *Crit. Rev. Biotechnol.* **27**, 197–216.
Dias, F. M. V., Vincent, F., Pell, G., Prates, J. A. M., Centeno, M. S. J., Tailford, L. E., Ferreira, L. M. A., Fontes, C. M. G. A., Davies, G. J. & Gilbert, H. J. (2004). *J. Biol. Chem.* **279**, 25517–25526.
Dilokpimol, A., Nakai, H., Gotfredsen, C. H., Baumann, M. J., Nakai, N., Abou Hachem, M. & Svensson, B. (2011). *Biochim. Biophys. Acta*, **1814**, 1720–1729.
Ducros, V. M., Zechel, D. L., Murshudov, G. N., Gilbert, H. J., Szabó, L., Stoll, D., Withers, S. G. & Davies, G. J. (2002). *Angew. Chem. Int. Ed.* **41**, 2824–2827.
Emsley, P. & Cowtan, K. (2004). *Acta Cryst.* D**60**, 2126–2132.
Eneyskaya, E. V., Sundqvist, G., Golubev, A. M., Ibatullin, F. M., Ivanen, D. R., Shabalin, K. A., Brumer, H. & Kulminskaya, A. A. (2009). *Biochimie*, **91**, 632–638.
Gonçalves, A. M. D., Silva, C. S., Madeira, T. I., Coelho, R., de Sanctis, D., San Romão, M. V. & Bento, I. (2012). *Acta Cryst.* D**68**, 1468–1478.
Gouet, P., Robert, X. & Courcelle, E. (2003). *Nucleic Acids Res.* **31**, 3320–3323.
Hilge, M., Gloor, S. M., Rypniewski, W., Sauer, O., Heightman, T. D., Zimmermann, W., Winterhalter, K. & Piontek, K. (1998). *Structure*, **6**, 1433–1444.
Katrolia, P., Jia, H., Yan, Q., Song, S., Jiang, Z. & Xu, H. (2012). *Bioresour. Technol.* **110**, 578–586.
Katrolia, P., Yan, Q., Zhang, P., Zhou, P., Yang, S. & Jiang, Z. (2013). *J. Agric. Food Chem.* **61**, 394–401.
Kleywegt, G. J. (1999). *Acta Cryst.* D**55**, 1878–1884.
Krissinel, E. & Henrick, K. (2007). *J. Mol. Biol.* **372**, 774–797.
Laskowski, R. A. & Swindells, M. B. (2011). *J. Chem. Inf. Model.* **51**, 2778–2786.
Lombard, V., Golaconda Ramulu, H., Drula, E., Coutinho, P. M. & Henrissat, B. (2014). *Nucleic Acids Res.* **42**, D490–D495.
Lowry, O. H., Rosebrough, N. J., Farr, A. L. & Randall, R. J. (1951). *J. Biol. Chem.* **193**, 265–275.
Martín-Cuadrado, A. B., Fontaine, T., Esteban, P. F., del Dedo, J. E., de Medina-Redondo, M., del Rey, F., Latgé, J. P. & de Aldana, C. R. (2008). *Fungal Genet. Biol.* **45**, 542–553.
Mayer, J., Conrad, J., Klaiber, I., Lutz-Wahl, S., Beifuss, U. & Fischer, L. (2004). *J. Agric. Food Chem.* **52**, 6983–6990.
Moreira, L. R. & Filho, E. X. (2008). *Appl. Microbiol. Biotechnol.* **79**, 165–178.
Murshudov, G. N., Skubák, P., Lebedev, A. A., Pannu, N. S., Steiner, R. A., Nicholls, R. A., Winn, M. D., Long, F. & Vagin, A. A. (2011). *Acta Cryst.* D**67**, 355–367.
Otwinowski, Z. & Minor, W. (1997). *Methods Enzymol.* **276**, 307–326.
Park, S. H., Park, K. H., Oh, B. C., Alli, I. & Lee, B. H. (2011). *N. Biotechnol.* **28**, 639–648.
Petersen, T. N., Brunak, S., von Heijne, G. & Nielsen, H. (2011). *Nature Methods*, **8**, 785–786.
Reddy, S. K., Rosengren, A., Klaubauf, S., Kulkarni, T., Karlsson, E. N., de Vries, R. P. & Stålbrand, H. (2013). *FEBS Lett.* **587**, 3444–3449.
Rosengren, A., Hägglund, P., Anderson, L., Pavon-Orozco, P., Peterson-Wulff, R., Nerinckx, W. & Stålbrand, H. (2012). *Biocatal. Biotransformation*, **30**, 338–352.
Sabini, E., Schubert, H., Murshudov, G., Wilson, K. S., Siika-Aho, M. & Penttilä, M. (2000). *Acta Cryst.* D**56**, 3–13.
Sambrook, J. & Russell, D. W. (2001). *Molecular Cloning: A Laboratory Manual.* New York: Cold Spring Harbor Laboratory Press.
Santos, C. R. dos, Paiva, J. H., Meza, A. N., Cota, J., Alvarez, T. M., Ruller, R., Prade, R. A., Squina, F. M. & Murakami, M. T. (2012). *J. Struct. Biol.* **177**, 469–476.
Shi, H., Huang, Y., Zhang, Y., Li, W., Li, X. & Wang, F. (2013). *BMC Biotechnol.* **13**, 83.
Street, I. P., Kempton, J. B. & Withers, S. G. (1992). *Biochemistry*, **31**, 9970–9978.
Sweeney, M. D. & Xu, F. (2012). *Catalysts*, **2**, 244–263.
Tailford, L. E., Offen, W. A., Smith, N. L., Dumon, C., Morland, C., Gratien, J., Heck, M.-P., Stick, R. V., Blériot, Y., Vasella, A., Gilbert, H. J. & Davies, G. J. (2008). *Nature Chem. Biol.* **4**, 306–312.
Tankrathok, A., Iglesias-Fernández, J., Luang, S., Robinson, R. C., Kimura, A., Rovira, C., Hrmova, M. & Ketudat Cairns, J. R. (2013). *Acta Cryst.* D**69**, 2124–2135.
Teze, D., Hendrickx, J., Czjzek, M., Ropartz, D., Sanejouand, Y.-H., Tran, V., Tellier, C. & Dion, M. (2014). *Protein Eng. Des. Sel.* **27**, 13–19.
Vincent, F., Gloster, T. M., Macdonald, J., Morland, C., Stick, R. V., Dias, F. M. V., Prates, J. A. M., Fontes, C. M. G. A., Gilbert, H. J. & Davies, G. J. (2004). *Chembiochem*, **5**, 1596–1599.
Zhang, M., Jiang, Z., Li, L. & Katrolia, P. (2009). *J. Mol. Catal. B Enzym.* **60**, 119–124.
Zhou, P., Chen, Z., Yan, Q., Yang, S., Hilgenfeld, R. & Jiang, Z. (2013). *Acta Cryst.* D**69**, 2027–2038.
Zyl, W. H. van, Rose, S. H., Trollope, K. & Görgens, J. F. (2010). *Process Biochem.* **45**, 1203–1213.